Photoluminescence-Based Electron and Lattice Temperature Measurements in GaN-Based HEMTs

Jorge A. Ferrer-Pérez, Bruce Claflin, Debdeep Jena, Mihir Sen, Ramakrishna Vetury & Donald Dorsey

Journal of Electronic Materials

ISSN 0361-5235

Journal of Elec Materi
DOI 10.1007/s11664-013-2841-3

Springer

Your article is protected by copyright and all rights are held exclusively by TMS. This e-offprint is for personal use only and shall not be self-archived in electronic repositories. If you wish to self-archive your article, please use the accepted manuscript version for posting on your own website. You may further deposit the accepted manuscript version in any repository, provided it is only made publicly available 12 months after official publication or later and provided acknowledgement is given to the original source of publication and a link is inserted to the published article on Springer's website. The link must be accompanied by the following text: "The final publication is available at link.springer.com".

Springer

Author's personal copy

Journal of ELECTRONIC MATERIALS
DOI: 10.1007/s11664-013-2841-3
© 2013 TMS

Photoluminescence-Based Electron and Lattice Temperature Measurements in GaN-Based HEMTs

JORGE A. FERRER-PÉREZ,[1,6] BRUCE CLAFLIN,[2,7] DEBDEEP JENA,[3,8] MIHIR SEN,[1,9] RAMAKRISHNA VETURY,[4,10] and DONALD DORSEY[5,11]

1.—Department of Aerospace and Mechanical Engineering, University of Notre Dame, Notre Dame, IN 46556, USA. 2.—Air Force Research Laboratory, Sensors Directorate Wright–Patterson Air Force Base, Dayton, OH 45433, USA. 3.—Department of Electrical Engineering, University of Notre Dame, Notre Dame, IN 46556, USA. 4.—Defense and Power, RF Micro Devices, Inc., Charlotte, NC 28269, USA. 5.—Materials and Manufacturing Directorate, AFRL/RXAN, Wright–Patterson Air Force Base, Dayton, OH 45433, USA. 6.—e-mail: jferrerp@alumni.nd.edu. 7.—e-mail: Bruce.Claflin@wpafb.af.mil. 8.—e-mail: djena@nd.edu. 9.—e-mail: msen@nd.edu. 10.—e-mail: RVetury@rfmd.com. 11.—e-mail: Donald.Dorsey@wpafb.af.mil

Nitride-based semiconductors are gaining importance not only for high-power applications but also for high-temperature electronic devices. Using photoluminescence (PL) techniques, it is now possible to simultaneously determine the temperatures of the lattice and hot electrons in these devices. Therefore, it is possible to use PL mapping measurements to derive temperature profiles for electrons and the lattice in the active region of an operating device with a single set of measurements. This work presents an experimental process to construct such spatially resolved temperature maps for a planar semiconductor device under bias and applies this approach to a specific example using the conductive channels of a biased AlGaN/GaN high-electron-mobility transistor. Studying the temperature distribution inside the conductive channels will help understand how electrons flowing in the device interact with the lattice as well as the process of heat generation within the device.

Key words: Hot spots, hot-electron temperature, lattice temperature, photoluminescence, GaN HEMT, heat transfer

INTRODUCTION

GaN-based semiconductors have gained importance in electronic devices for high-speed and high-power applications, and for devices operating at high temperatures.[1,2] In addition, for applications in space they offer the additional advantage of radiation hardness, and have improved survivability in the hazardous space environment.[3,4] However, for both terrestrial- and space-based applications, sustained high-temperature operation can degrade the semiconductor device performance and ultimately impact the device reliability.[5] Miniaturization also plays a role, since it results in a significant increase in the power density within the device.[6] The higher current densities in these devices produce more localized Joule heating as the electrons transfer energy to phonons through lattice scattering.[7] These localized heating sources, or hot spots, have been studied in the past numerically[8] and experimentally.[9] Also, there are efforts designed to cool devices by adding new structures during the fabrication process.[10,11] It is clear that managing the thermal budget of the device by minimizing heat generation depends on understanding these electron–phonon interactions in detail.

To determine the behaviors of electron and lattice temperatures in the active region of GaN-based high-electron-mobility transistors (HEMTs), several experimental approaches, including luminescence techniques,[12] have been utilized. Depth-resolved microcathodoluminescence spectroscopy was used to study the thermal distribution and defect generation

(Received November 27, 2012; accepted October 7, 2013)

Published online: 23 November 2013

Author's personal copy

inside an operating HEMT without distinction between the lattice and electron temperatures.[13] Furthermore, electroluminescence (EL) measurements under bias condition have helped understand the degradation and reliability of HEMT devices, where EL peak intensity is a good indicator of the hot-electron concentration.[14] From EL measurements hot-carrier temperatures can be extracted using the high-energy tail (HET).[15] Lattice temperatures have also been extracted from microphotoluminescence (μ-PL) measurements using the Varshni equation across a cut in the channel.[16] In addition, spatially resolved lattice temperatures along a cut in the channel have been compared with finite-element numerical calculations.[17] Care must be exercised when performing these measurements to limit the excitation laser power on biased devices to avoid self-heating or photoinduced channel current, which can distort the results[18] and significantly degrade the device.

Although electron temperatures from point locations in AlN/GaN-based HEMTs[19,20] have been extracted using PL measurements, spatially resolved two-dimensional (2-D) electron temperature maps have not been reported. In contrast, 2-D lattice temperature maps have been derived from separate PL and Raman measurements using the same InAl(Ga)N/GaN HEMT device, under identical operating conditions. These measured thermal profiles were compared with infrared (IR) images as well as with numerical simulations[21] to show the equivalence of both approaches while also noting the relative advantages, limitations, and challenges associated with each technique. The present work demonstrates an experimental procedure to simultaneously generate 2-D electron and lattice temperature maps in GaN-based HEMTs from a set of PL measurements only. Such maps provide direct spatial visualization of the electron and lattice temperature distributions and hot-spot formation in GaN-based HEMTs from PL measurements under different operating conditions.

The construction of these temperature maps proceeds in two stages. In the first stage, measurements are performed on an unbiased device to verify the methodology. Since no voltage is applied, the electron and lattice temperatures are expected to be the same. Measured parameters for the Varshni equation can be extracted from these unbiased data, providing a temperature calibration that can be subsequently applied to devices under bias. The second stage consists of PL measurements on a biased device where electron and lattice temperature profiles for the entire active region are mapped.

EXPERIMENTAL PROCEDURES

Experiments with different incident laser power intensities ranging from 10 μW to 2000 μW were performed at room temperature on a specially engineered two-finger 400-μm-gate-width (2×200 μm) AlGaN/GaN HEMT device with $\sim$20 μm of open channel between gate and drain to facilitate optical studies. The layered stack consisted of an AlGaN barrier structure, a 2-μm GaN buffer layer, and a nucleation layer on a semi-insulating SiC substrate that was thinned to 100 μm. Confocal μ-PL measurements in backscattering geometry were made using $\lambda_0 = 325$ nm HeCd laser excitation. A 39$\times$ ultraviolet (UV) objective focused the laser to a $\sim$3-μm-diameter spot, and the PL spectra were collected with a Si charge-coupled device (CCD) array. Neutral-density filters were used to vary the incident laser intensity.

The resulting spectra can be grouped qualitatively into three power ranges: low ($P_I < 100$ μW), medium (100 μW $\leq P_I < 1000$ μW), and high (1000 μW $< P_I$), as shown in Fig. 1.

Electron and lattice temperatures were extracted from the PL spectra as described below. The electron temperature, T_e, is related to the HET of the PL spectra, which follows an exponential decay given by Ref. 22,23 as

$$I_{PL}^{HET} \propto \left[\exp\left(-\frac{E-E_g}{k_B T_e}\right)\right], \quad (1)$$

in the nondegenerate carrier approximation. From the logarithm of the PL spectrum, the slope m of the HET is related to the electron temperature by $m = 1/k_B T_e$. Minimizing the error given by

$$\text{Error} = \sum \left[I_{PL} - I_{PL}^{HET}\right]^2, \quad (2)$$

T_e is extracted.

The lattice temperature, T_L, is determined from the PL peak energy, E_p, using the Varshni equation[24]

$$E_p = E(0) - \frac{\Upsilon T_L^2}{T_L + \Delta}. \quad (3)$$

Equation 3 is solved for T_L, and the positive root is chosen.

Since the Varshni equation is an empirical relation,[25] the coefficients $E(0)$, Υ, and Δ can be derived experimentally for the specific apparatus used for the measurements to improve the accuracy of the lattice temperature calculations. Specifically, the sample was heated with a resistive heater block and the temperature was allowed to stabilize for at least 1 h. Reference PL spectra were recorded in 25°C steps from 25°C to 175°C, and peak energies for each spectra were determined from least-squares fits to Voigt profiles. Coefficients for the Varshni equation were determined from least-squares fits to these data.

Finally, confocal μ-PL maps were recorded with 1 μm spatial resolution over a 200 μm $\times$ 200 μm area which included the active region of the same HEMT device described above. The drain voltage V_d and drain current I_d were fixed at 10 V and 177 mA,

Author's personal copy

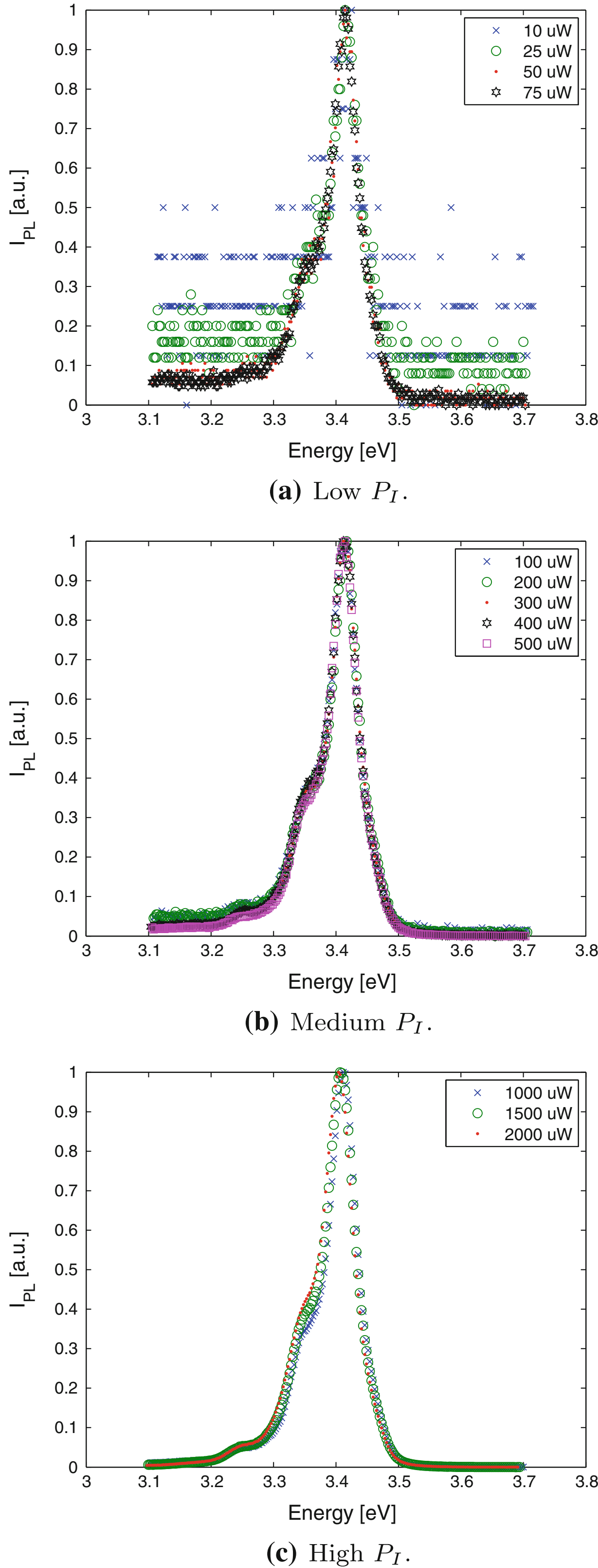

(a) Low P_I.

(b) Medium P_I.

(c) High P_I.

Fig. 1. Collected PL for three different ranges of P_I normalized.

respectively, and the analysis procedures detailed above were used to determine electron and lattice temperatures.

RESULTS

The coefficients of the Varshni equation $E(0)$, Υ, and Δ were determined using reference PL spectra from the unbiased device, measured as a function of laser intensity for a number of different fixed temperatures, T_p. Modulation in T_p affects the measured PL energy peak E_p as shown in Fig. 2. Note that the error bars for the energy peak (not shown for clarity) are ~14 meV.

For a particular incident laser intensity P_I, nonlinear regression can be applied between Eq. 3 and the experimental data to extract the values of $E(0)$, Υ, and Δ. To provide adequate signal to noise while minimizing laser-induced heating effects, $P_I = 10\ \mu$W was used to obtain the following values: $\Upsilon = 5.168 \times 10^{-4}$ eV/K and $\Delta = 141.9$ K. Note that the literature value of $E(0) = 3.510$ eV for GaN was used to decrease the complexity of the nonlinear regression calculations. Figure 3 shows the difference between T_L and T_p for different incident laser intensities using the derived values of the Varshni coefficients determined above. As expected $T_p \approx T_L$, with a maximum difference in the temperatures of ~15 K. The error bars for T_L are ~33 K (not shown).*

Note that the shifts in the PL peak energy with temperature are small, which makes the use of this method to determine the temperature extremely sensitive to the coefficients of the Varshni equation. Because of this sensitivity, and because these coefficients are not fundamental materials quantities but reflect the characteristics of the specific measurement equipment used, a detailed calibration of the apparatus used in this experiment was performed as described above. The difference between lattice temperatures calculated from two sets of Varshni coefficients, namely literature values and derived as shown in Fig. 4, clearly demonstrates the need for such care in analyzing the data and the error that can be introduced by using a "calibration" based on literature values of the Varshni coefficients.

Figure 4 shows a comparison between the electron and lattice temperatures for different values of P_I at room temperature. When the electron and lattice temperatures were compared, the maximum difference was <25 K. Electron temperatures derived from low-P_I (10 μW and 25 μW) data were unreasonably high because of the large amount of scatter in the data. Likewise, it is important to note that high intensities are undesirable because laser self-heating can distort the temperature calibration, resulting in inaccurate determination of temperature values when applied to biased devices. Therefore, it is critical to strike a balance between the need for a good signal-to-noise ratio while minimizing laser-induced heating effects.

*See Appendix for the full procedure for the calculation of error bars for lattice and electron temperatures.

Author's personal copy

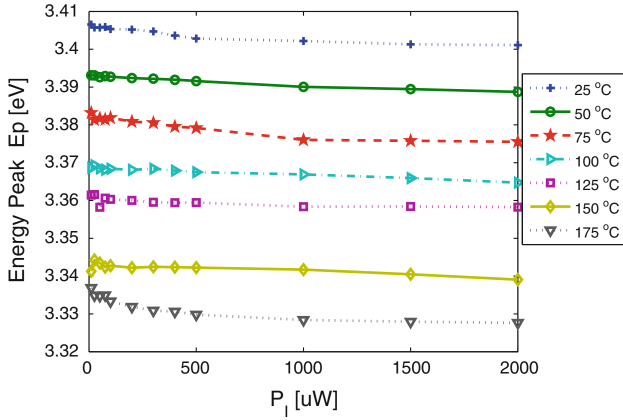

Fig. 2. Energy peak variation versus P_I for different values of T_p.

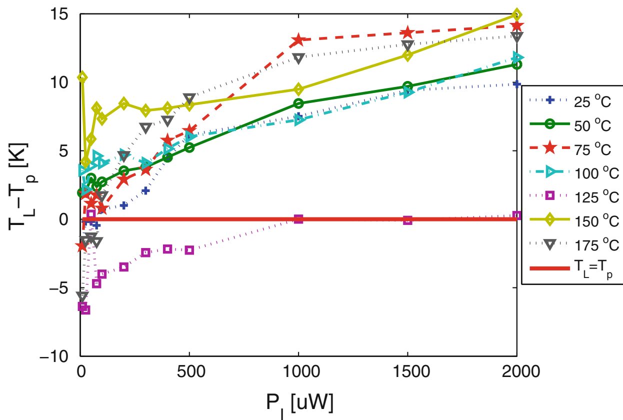

Fig. 3. Difference between T_L and T_p for different incident laser intensities using the derived values of the Varshni coefficients: $E(0) = 3.510$ eV, $\Upsilon = 5.168 \times 10^{-4}$ eV/K, and $\Delta = 141.9$ K.

Having verified the experimental measurement methodology by showing agreement between the electron and lattice temperatures in the unbiased device, measurements were performed on the same device under direct-current (DC) biased conditions. Care was taken to limit the incident laser power because excessive photogenerated carriers can substantially modify the operation of the device, making the PL measurements invasive. Although there was a slight increase in I_d (∼3%) with the laser ON, the impact of photogenerated carriers should be minimal for the low P_I values reported here. Using similar operating conditions, Batten et al.[18] found less than 5°C laser-induced heating. This temperature increase is within the error bars for this measurement. The laser power directed at the sample was kept low to minimize possible degradation of the device during measurement. Degradation was observed in other devices (not shown) during the course of measurement when supplying higher laser power to the sample; these effects include a significant and irreversible increase in I_d as well as increased temperature in the channel. No significant

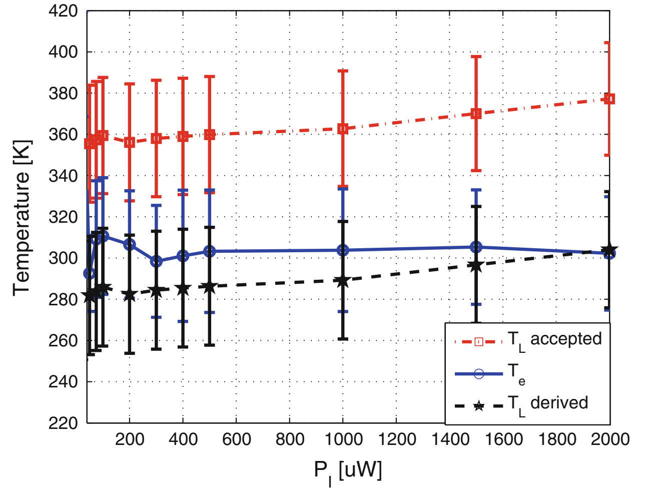

Fig. 4. Comparison of electron temperature versus lattice temperature using the accepted values of GaN and using the derived coefficients of the Varshni equation.

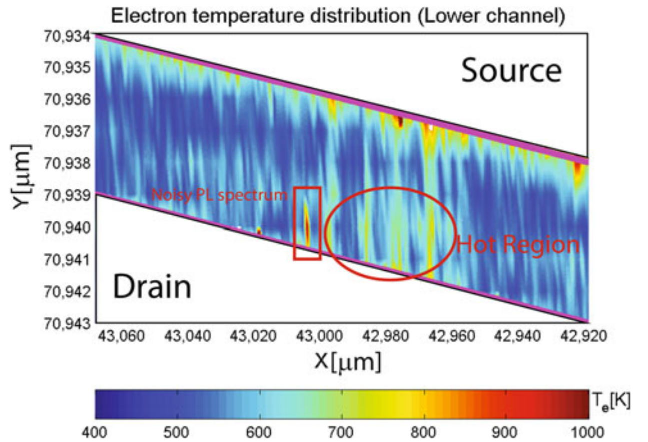

Fig. 5. Electron temperature map.

degradation effects were observed during the course of the measurement reported here.

When the device is ON, electrons start to flow and collisions between them or with the atoms of the crystal can occur. Depending on the energy of the electrons, they can absorb or emit phonons. If the electrons are very energetic and the phonon emission rate is higher than the phonon absorption rate, then the energy coming from the electrons will be transmitted to the lattice. These *hot phonons* that were launched by energetic *hot electrons* remain localized in the regions where electrons flow. Since LO phonons have small group velocity, they tend to accumulate and store energy, and as a consequence heat is generated.[26] To remove this heat, hot phonons need to decay through other vibrational modes. For GaN, it was proposed that LO modes change into LA+TO modes.[27] For GaN-based HEMTs, the hot-phonon lifetime in the two-dimensional electron gas channel is ∼350 fs, which is 35 times longer

Author's personal copy

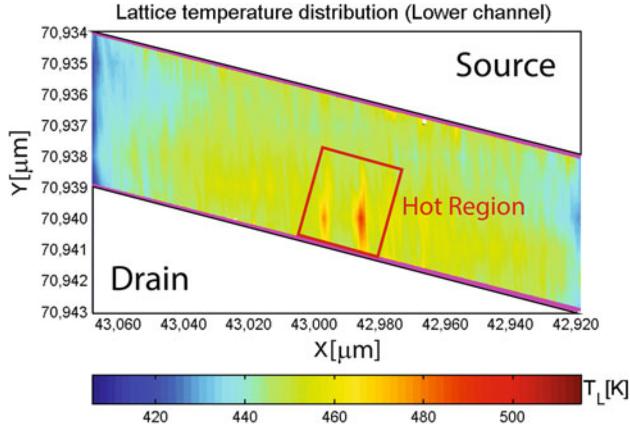

Fig. 6. Lattice temperature map.

than the lifetime of spontaneous LO phonons (∼10 fs). This difference in their lifetime causes an accumulation of heat in the channel.[28] Since the device is operating in an open-channel bias regime, electrons traveling from source to drain are accelerated by high electric fields. This fact increases the probability that hot electrons will collide with the lattice. These scattering events transmit energy to LO phonons, generating heat as stated above. For this reason, hot spots are expected to be localized close to the drain contact. A hot spot is observed in the electron temperature map in the active region shown in Fig. 5. The corresponding lattice temperature map shown in Fig. 6 includes a well-defined hot strip close to the drain as expected, as well as hot spots in the same region where the electron hot spots are observed.

CONCLUSIONS

This work provides a general procedure to construct simultaneous electron and lattice temperature maps for the active region of a planar semiconductor device under bias using only PL measurements. Electron and lattice temperatures, T_e and T_L, can be extracted with reasonable accuracy, by fitting the HET of experimental PL spectra to a theoretical model given by Eq. 1 and using a Varshni equation fit to the peak energy, respectively. This process was applied to an AlGaN/GaN HEMT device. For the unbiased device, values for the Varshni equation coefficients $E(0) = 3.510\,\text{eV}$, $\Upsilon = 5.168 \times 10^{-4}\,\text{eV/K}$, and $\Delta = 141.9\,\text{K}$ were derived from experimentally measured reference PL spectra collected between 25°C and 175°C. Three different ranges of P_I were tested in experiments: low, medium, and high. For each of these ranges, the PL emission spectrum was collected and electron temperatures were extracted. The measured values satisfied $T_e \approx T_L$, as expected since the experiments were performed on an unbiased AlGaN/GaN HEMT device. The accuracy in the extraction of these temperatures depends strongly on the scatter in the data. For low values of incident laser power intensity (10 μW and 25 μW), the electron temperature values determined are unreasonably high. The inclusion of the low-power data is important to establish a lower limit on the incident laser power that can be reliably used for the PL measurements. It is desirable to minimize the incident power to avoid laser-induced heating problems. Excluding these low values of P_I, the maximum error measured between lattice and electron temperatures was < 25 K. As P_I is increased, the signal-to-noise ratio of the experimental data improves, but laser-induced heating results in a redshift of the peak energy. This shift translates into a small increase in the apparent lattice temperature. Since no bias is applied, there is no convection due to electron flow, and conduction is the main mechanism of heat transfer. Nevertheless it is necessary to limit P_I values because the high density of photogenerated carriers can substantially modify the operation of a biased device or even degrade its performance significantly, making the PL measurements invasive.

For a DC biased device, electron and lattice temperatures were extracted from PL spectra and spatially resolved temperature maps were obtained. When a bias is applied, it is possible to observe the formation of hot regions close to the drain as expected. Such temperature maps are a valuable tool to visualize hot regions when the device is operating, and they can help to understand the interaction of electrons with the lattice and the local process of heat generation.

ACKNOWLEDGEMENTS

J.A.F.-P. is grateful for a scholarship from CONACYT-Mexico, and also expresses his gratitude to Dr. Vladimir Protasenko, Dr. Gregg Jessen, and Dr. Eric Heller for discussions and help. The work of B.C. was partially supported by AFRL Contract #FA8650-06-D-5401.

APPENDIX

This appendix describes the procedure for calculation of the error bars for the electron and lattice temperatures.

The electron temperature is given by

$$m = \frac{1}{k_B T_e}, \tag{4}$$

where m is the slope obtained from the logarithm of the PL spectrum, i.e., $\ln(I_{PL})$ versus E. The uncertainty in the determination of m is[29]

$$\delta m = \left| -\frac{1}{k_B T_e^2} \right| \delta T_e, \tag{5}$$

Author's personal copy

where δm is the standard deviation of the slope. For brevity, we use X and Y to represent the N elements of E and $\ln(I_{\mathrm{PL}})$, respectively. Therefore,[30]

$$\delta m^2 = \left[\sum_{j=1}^{N}\left(\frac{\partial m}{\partial X_j}\right)^2\right]s_X^2 + \left[\sum_{j=1}^{N}\left(\frac{\partial m}{\partial Y_j}\right)^2\right]s_Y^2. \quad (6)$$

The standard deviations of X and Y are given by

$$s_X^2 = \frac{\sum_1^N \delta X_i}{N}, \qquad s_Y^2 = \frac{\sum_1^N \delta Y_i}{N-2}, \quad (7)$$

where the uncertainty expressions for δX_i and δY_i are

$$\delta X_i = \left| -\frac{1239.5}{\lambda_i^2} \right| \delta\lambda_i, \qquad \delta Y_i = \frac{\delta I_i}{I_i}. \quad (8)$$

Since m is given by

$$m = \frac{N\sum_i^N (X_i Y_i) - \sum_i^N X_i \sum_i^N Y_i}{N\sum_i^N X_i^2 - \left(\sum_i^N X_i\right)^2}, \quad (9)$$

then

$$\frac{\partial m}{\partial X_j} = \frac{1}{\left(N\sum_i^N X_i^2 - \left(\sum_i^N X_i\right)^2\right)^2} \left[\left(N\sum_i^N X_i^2 - \left(\sum_i^N X_i\right)^2\right)\left(NY_j - \sum_i^N Y_i\right) - \left(N\sum_i^N X_i Y_i - \sum_i^N X_i \sum_i^N Y_i\right)\left(2NX_j - 2\sum_i^N X_i\right)\right] \quad (10)$$

and

$$\frac{\partial m}{\partial Y_j} = \frac{NX_j - \sum_i^N X_i}{N\sum_i^N X_i^2 - \left(\sum_i^N X_i\right)^2}. \quad (11)$$

Finally, using Eqs. 7–11, δm can be calculated from Eq. 6 and δT_{e} can be found from Eq. 5. Then, the error bars for the electron temperature are given by $\pm\delta T_{\mathrm{e}}$.

The lattice temperature is determined using the Varshni equation

$$E_{\mathrm{P}} = E(0) - \frac{\Upsilon T_{\mathrm{L}}^2}{T_{\mathrm{L}} + \Delta}. \quad (12)$$

From Eq. 12, it is trivial to show that

$$\delta T_{\mathrm{L}} = \left| -\frac{\Delta + T_{\mathrm{L}}}{2\Upsilon T_{\mathrm{L}} + E_{\mathrm{P}} - E(0)} \right| \delta E_{\mathrm{P}}. \quad (13)$$

Therefore, the error bars for the lattice temperature are given by $\pm\delta T_{\mathrm{L}}$.

REFERENCES

1. M.S. Shur and R.F. Davis, *GaN-Based Materials and Devices,* 1st edn. (Singapore: World Scientific, 2004), pp. 225–244.
2. T. Steiner, *Semiconductor Nanostructures for Optoelectronic Applications,* 1st edn. (Norwood, MA: Artech House, 2004), pp. 19, 289–344.
3. A.R. Barnes, A. Boetti, L. Marchand and J. Hopkins, (Paper presented at 13th European Gallium Arsenide and Other Compound Semiconductors Application Symposium EGA-AS, Paris, 3–4 October 2005).
4. M.A.G. Darrin, S.P. Buchner, and M. Martin, (Paper presented at 8th European Conference on Radiation and Its Effects on Components and Systems RADECS, Cap d'Agde, 19–23 September 2005).
5. R. Quay, *Gallium Nitride Electronics,* 1st edn. (Berlin, Germany: Springer, 2008), pp. 311–336.
6. F.J. Pollack, (Paper presented at 32nd Annual International Symopsium on Microarchitecture MICRO-32, Haifa, 16–18 November 1999).
7. A. Matulionis, J. Liberis, I. Matulioniene, E. Sermuksnis, J.H. Leach, M. Wu, and H. Morkoc, *Phys. Status Solidi A* 208, 30 (2011).
8. A. Majumdar, K. Fushinobu, and K. Hijikata, *J. Appl. Phys.* 77, 6686 (1995).
9. J. Bolte, F. Niebisch, J. Pelzl, P. Stelmaszyk, and A.D. Wieck, *J. Appl. Phys.* 84, 6917 (1998).
10. P. Wang and A. Bar-Cohen, *J. Appl. Phys.* 102, 11 (2007).
11. Y. Zhang, G. Zeng, C. Hoffman, A. Bar-Cohen, and A. Shakouri, *IEEE Trans. Compon. Packag. Technol.*, 31, 552 (2008).
12. C.F. Lo, F. Ren, S.J. Pearton, A.Y. Polyakov, N.B. Smirnov, A.V. Govorkov, I.A. Belogorokhov, A.I. Belogorokhov, V.Y. Reznik, and J.W. Johnson, *J. Vac. Sci. Technol. B*, 29, 4 (2011).
13. C.H. Lin, T.A. Merz, D.R. Doutt, M.J. Hetzer, J. Joh, J.A. del Alamo, U.K. Mishra, and L.J. Brillson, *Appl. Phys. Lett.,* 95, 3 (2009).
14. G. Meneghesso, G. Verzellesi, F. Danesin, F. Rampazzo, F. Zanon, A. Tazzoli, M. Meneghini, and E. Zanoni, *IEEE Technol. Device Mater. Reliab.,* 8, 332 (2008).
15. M. Tapajna, R.J.T. Simms, Y. Pei, U. Mishra, and M. Kuball, *IEEE Electron Device Lett.,* 31, 7 (2010).
16. M. Gonschorek, D. Simeonov, J.F. Carlin, E. Feltin, M.A. Py, and N. Grandjean, *Eur. Phys. J. Appl. Phys.,* 47, 3 (2009).
17. N. Shigekawa, K. Onodera, and K. Shiojima, *Jpn. J. Appl. Phys.,* 42, 2245 (2003).
18. T. Batten, A. Manoi, M.J. Uren, T. Martin, and M. Kuball, *J. Appl. Phys.,* 107, 174502 (2010).
19. S.K. Tripathy, G. Xu, X. Mu, Y.J. Ding, K. Wang, Y. Cao, D. Jena, and J.B. Khurgin, *Appl. Phys. Lett.,* 92, 3 (2008).
20. G. Xu, S.K. Tripathy, X. Mu, Y.J. Ding, K. Wang, Y. Cao, D. Jena, and J.B. Khurgin, *Laser Phys.,* 19, 745 (2009).
21. B. Claflin, E.R. Heller, B. Winningham, J.E. Hoelscher, M. Bellott, K. Chabak, A. Crespo, J. Gillespie, V. Miller, M. Trejo, G.H. Jessen, and G.D. Via (Paper presented at CS MANTECH Conference, Tampa, 18–21 May 2009).
22. J. Shah, A. Pinczuk, C. Gossard, and W. Wiegmann, *Phys. Rev. Lett.,* 54, 2045 (1985).
23. K. Wang, J. Simon, N. Goel, and D. Jena, *Appl. Phys. Lett.,* 88, 3 (2006).

Author's personal copy

24. I. Vurgaftman and J.R. Meyer, *J. Appl. Phys.,* 94, 3675 (2003).
25. Y.P. Varshni, *Physica,* 34, 149 (1967).
26. A. Matulionis, J. Liberis, I. Matulioniene, E. Sermuksnis, J.H. Leach, M. Wu, and H. Morkoc, *Phys. Status Solidi A,* 208, 30 (2011).
27. B.K. Ridley, *J. Phys. Condens. Mater.,* 8, L511 (1996).
28. A. Matulionis, *Phys. Status Solidi A,* 203, 2313 (2006).
29. S.J. Kline and F.A. McClintock, *Mech. Eng.,* 75, 3 (1953).
30. D.C. Baird, *Experimentation: An Introduction to Measurement Theory and Experiment Design,* 2nd edn. (Prentice Hall, NJ: Englewood Cliffs, 1988), pp. 172–177.